RSC Advances

ROYAL SOCIETY OF CHEMISTRY

www.rsc.org/advances

Journal Name

ARTICLE

Effect of the MWCNTs selective localization on the dielectric properties for PVDF/PS/HDPE ternary blends with in-situ formed core-shell structure

Received 00th January 20xx,
Accepted 00th January 20xx

DOI: 10.1039/x0xx00000x

www.rsc.org/

Shuang-lin Li, Rui Dou, Yan Shao, Bo Yin*, Ming-bo Yang

This work demonstrated the selective localization of multiwall carbon nanotubes (MWCNTs) in (70/20/10 vol%) poly(vinylidene fluoride) (PVDF)/poly(styrene) (PS)/high-density poly(ethylene) (HDPE) ternary blends to be an effective method to reduce the dielectric loss and maintain high dielectric constant simultaneously. Here, PVDF/PS/HDPE blends displayed a core-shell structure, HDPE phase was the core and PS phase was the shell. When MWCNTs was added into PVDF/PS/HDPE blends, it stably dispersed in the PS layer. The morphology, electrical properties, and dielectric properties of (PVDF/PS/HDPE)/MWCNTs composites were investigated. The results indicated that the conductivity as well as the dielectric permittivity value increased with the content of MWCNTs. Meanwhile, the dielectric permittivity was dependent on the electric field frequency. The dielectric constant for (PVDF/PS/HDPE)/MWCNTs composites was 400 with 1.0 vol% MWCNTs at 10^2 Hz, accompanied by a low dielectric loss of 10 which was about 400 times lower than that of PVDF/MWCNTs composites. Therefore, a low dielectric loss and high dielectric constant for (PVDF/PS/HDPE)/MWCNTs composites, which formed a core-shell structure, have been obtained through MWCNTs selectively locating in PS shell even at high contents of MWCNTs.

Introduction

In recent years, there has been a great interest in developing polymer-based dielectric materials with high dielectric constant and low dielectric loss owing to their potential application such as electric energy storage devices, artificial muscles, and sensors.[1-3] As we know, polymers are most promising materials due to their high mechanical properties, good processability, light weight, and low cost. However, the dielectric constant of the pure polymers is usually quite low, which restricted the application of polymers as dielectric materials. To improve the dielectric constant of polymers, one common approach is to add ceramics powder with high dielectric constant, such as $BaTiO_3$.[4, 5] Unfortunately, to get a higher dielectric constant, the high loading of ceramic fillers is required, which results in the deterioration of the mechanical, processing properties, and high cost. Another widely used strategy is to add conductive fillers into the matrix. Conductive fillers such as carbon nanotubes (CNTs), carbon black (CB), carbon fibers (CFs), and graphene oxide (GO) have been widely used in polymer-based composites to improve the electrical, mechanical or thermal properties of the materials.[6-8] Among these conductive fillers, CNTs exhibits excellent electrical properties and unique mechanical properties due to its high aspect ratio. Compared with ceramic/polymer composites, a small content of CNTs is sufficient to obtain a high dielectric constant.[9-11] Normally, CNTs/polymer composites are good conductive ones but not good for dielectrics because the large increase in dielectric constant of the composites is usually accompanied by a dramatic increase in dielectric loss, which largely limits their practical application.[12, 13]

As we know, the CNTs/polymer composites become conductive not dielectric if CNTs contact with each other. Thus, attempts have been made to reduce dielectric loss (tan δ) by introducing interlayers or insulating shells on the conductive fillers to prevent them from connecting each other directly.[14] Yang et al. [15] have reported that the composites with a stable high dielectric constant (~44) and rather low dielectric loss (<0.07) were prepared. The largely-enhanced dielectric performance originated from the organic shell polypyrrole (PPy) of multiwall carbon nanotubes (MWCNTs) through the inverse microemulsion polymerization. As a result, the organic shell not only ensured good dispersion of MWCNTs in the matrix, and also screened charge movement to shut off leakage current. Chen et al. [16] prepared a sandwich multi-layer structure polymer-based dielectrics with a dielectric layer (NH_2-MWNT/PI composites) intercalated between insulating layers (pure PI). When the filler content of the mid-layer is 10 wt%, the composites have the highest dielectric constant of 31.3-30.5 and rather low dielectric loss of 0.0016-0.022 between the frequencies of 1 to 1MHz. The fillers selectively locate in one phase of the composites, which can provide interlayers or insulating shells for fillers to prevent them from the direct connection. Zhao et al. [17]

College of Polymer Science and Engineering, State Key Laboratory of Polymer Materials Engineering, Sichuan University, Chengdu, Sichuan, People's Republic of China.
E-mail: yinbo@scu.edu.cn; Fax: +86-28-85405324; Tel:+86-28-85405324

tuned the dielectric properties of immiscible PS/PVDF blends by selectively localizing carbon black (CB) nanoparticles in different phases. What's more, Zhao et al. [18] have successfully prepared the nanocomposites with ultra-low percolation threshold and high dielectric performance by controlling the selective distribution of MWCNTs in the poly(methyl methacrylate) (PMMA) shell of PS/PMMA/PVDF ternary continuous polymer blends. In addition, the composites' dielectric properties show excellent temperature stability. Therefore, the selective distribution of fillers in the one phase of the immiscible polymer composites is an effective method to achieve high performance dielectric material.

In recent years, the ternary polymer blends, presented a wide variety of micro-structured morphologies with multiple interfaces between different phases, attracted more attention.[19-21] For ternary polymer blends, complete wetting and partial wetting are two categories of morphological states. The spreading theory, defined by Harkins equation, was employed to describe complete and partial wetting. Hobbs et al. [22] rewrote Harkins equation and calculated three spreading coefficients of ternary polymers system to predict the morphology of the blends. In a ternary blend of three polymers *A, B*, and *C*, (supposing *A* is the matrix) the spreading coefficient,

$$\lambda_{BC} = \gamma_{AC} - \gamma_{AB} - \gamma_{BC} \quad (1)$$

where γ values are the interfacial tensions between the different phases. The spreading coefficient, λ_{BC}, shows the tendency of component *B* to encapsulate or spread onto phase *C*. In a certain ternary blend, three different spreading coefficients exist including $\lambda_{BC}=\lambda_{BA}$, $\lambda_{AB}=\lambda_{AC}$, and $\lambda_{CA}=\lambda_{CB}$. A positive value of one of the spreading coefficients demonstrates that the complete wetting behavior will be observed. A matrix/core-shell dispersed phase structure is an example of the complete wetting. For example, if λ_{BC} is positive indicates that phase *B* encapsulates dispersed phase *C* in the matrix of *A* as shown in Fig. 1a. In the case that all three spreading coefficients are negative, a partial wetting will be observed in which none of the phases locates fully between the two others as shown in Fig. 1b.

Although considerable works have been done to design the polymer-based dielectric materials with high dielectric constant and low dielectric loss filled with various fillers, to the best of our knowledge, there are still lack of sufficient studies on the influence of the fillers selective localization at three immiscible polymers which can obtain the core-shell structure. In the current study, the main purpose is to obtain MWCNTs/polymer composites with high dielectric constant and a low dielectric loss by introducing the core-shell structure and MWCNTs selectively locating in the shell layer. The core-shell structure was obtained in the composition (70/20/10 vol%) of PVDF/PS/HDPE composites. PVDF, with high dielectric constant, mechanical strength, thermal stability and chemical stability, is commonly accepted as an ideal matrix for the fabrication of dielectric composites.[23-25] The influence of MWCNTs loading on the morphology, electrical properties, and dielectric properties of the (PVDF/PS/HDPE)/MWCNTs composites will be systematically investigated and discussed in this article.

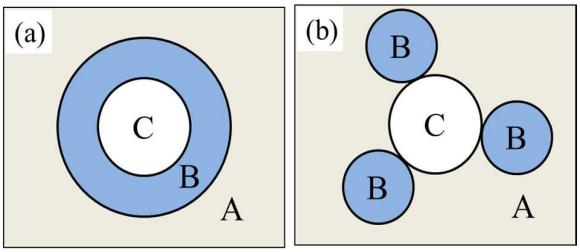

Fig.1 Equilibrium morphologies for ABC ternary polymer blends (a) complete wetting: the case that one phase locates between two other phases, and (b) partial wetting: the case that all phases are in contact with each other.

Experimental section

Materials

PVDF (type FR906) powder with density of 1.6 g/cm^3 at 200 ℃ was purchased from Shanghai 3F New Materials Company (China). PS (type PG-33) pellets with density of 0.95 g/cm^3 at 200 ℃ was purchased from Taiwan Qimei Company. HDPE (type 5000s) pellets with density of 0.85g/cm^3 at 200℃ was purchased from Lanzhou Chemical Industry (Lanzhou, China). MWCNTs (type NC7000), average diameter of 10 nm and length of 1.5 μm and specific surface area of 250-300m^2 g^{-1}, was supplied by Nanocyl S. A. (Belgium).

Sample preparation

All the polymers were dried in a vacuum oven at 60 ℃ overnight before blending. For the preparation of (PVDF/PS/HDPE)/MWCNTs nanocomposites, the volume ratios of PVDF/PS/HDPE fixed as 70/20/10 vol%, and varied the volume fraction of MWCNTs. All components were added into the HAAKE torque rheometer (XSS-300) at 200 ℃ and with screw speeds of 100 rpm for 8 min simultaneously. The samples were marked as *SMx*, and *x* represented the loading of MWCNTs. As the comparison group, PVDF/MWCNTs nanocomposites used the same method to prepare, the samples were marked as *VMy*, and *y* represented the content of MWCNTs. After blending, the mixtures were molded by hot pressing at 200 ℃ and 10 MPa for further characterizations. The volume fraction of MWCNTs given below was relative to the whole system.

Characterization

Interfacial Tension Measurement

The interfacial tension for polymers pairs in this study was determined using the rheological behaviour of their respective blends. And the data were analysed using Gramespasher and Meissner's analyses.[26, 27]

Electrical Conductivity

The direct current conductivity (σ_{DC}) measurement of the composites was done by a Keithley 6517B electrometer (Keithley Instruments, Ohio) on the molded specimen bars of dimensions 30 × 10 × 2 mm^3. Prior to the measurements, electrodes of silver were

pasted on the opposite sides of samples. Minimum of five tests were performed for each specimen and the data was averaged.

The alternating current conductivity (σ_{AC}) of the composites (disc type sample with thickness ~ 2.7 mm and diameter ~ 20 mm) was obtained using Agilent 4294A precision LCR meter in the frequency (f) region of 100 Hz to 10MHz at room temperature.

Dielectric measurement

The value such as parallel capacitance (C_p) and dielectric loss tangent (tan δ) were also obtained as a function of f using the Agilent 4294A precision LCR meter. The dielectric constant (ε) was determined with the following equation:

$$\varepsilon = \frac{C_p}{C_0} \quad (2)$$

where C_p is the observed capacitance of the sample, and C_0 ($= \varepsilon_0 A/d$) is the capacitance with vacuum between parallel plates, and ε_0 is vacuum permittivity, A is the area of electrodes, and d is the thickness of the samples.

Morphology Observation

The samples were fractured in liquid nitrogen and then the fractured surface was directly sputtered with a thin layer of gold. Morphology observation was performed at an accelerating voltage of 20.0 kV using a JEOL JSM-5900LV scanning electron microscopy (SEM, JEOL, Japan).

The dispersion states of MWCNTs in the nanocomposites at the microcosmic scale were observed with transmission electron microscope (TEM, Philips CM120) equipped with field emission gun (FEG) at 200 kV. Ultrathin sample sections with a thickness of 100 nm were cut on a Leica EM UC6 ultramicrotome (Leica Microsystems, Wetzlar, Germany) at −150 ℃.

Results and discussion

Matrix/core-shell dispersed phase morphology

The interfacial tension values and the spreading coefficients of polymer pairs for the ternary PVDF/PS/HDPE systems at 200 ℃ are reported in Table 1. For ternary blend of PVDF/PS/HDPE, the high interfacial tension of HDPE/PVDF ($\gamma_{HDPE/PVDF}$ = 11.9), and the low interfacial tension of PVDF/PS ($\gamma_{PS/HDPE}$ = 4.7) and PS/HDPE ($\gamma_{PS/HDPE}$ = 3.4), resulting in a positive spreading coefficient of PS over HDPE ($\lambda_{PS/HDPE}$) with a value of 3.8 mN/m. The other two spreading coefficients are negative, they are $\lambda_{PVDF/PS}$ = −13.2 mN/m and $\lambda_{HDPE/PVDF}$ = −10.6 mN/m, respectively. This predicts a complete wetting case with the development of a thermodynamically stable PS layer between PVDF and HDPE. The sketch map of core-shell morphology is shown in Fig. 2a. Fig. 2b, c and d show the real phase morphology of PVDF/PS/HDPE (70/20/10 vol%) ternary blends. The spherical structure can be clearly observed in Fig. 2b. In order to distinguish the phases, PS is etched by xylene as shown in Fig. 2c and d. The cracks between PVDF and HDPE phases can be clearly observed in contrast to Fig. 2b. This demonstrates that HDPE is encapsulated by PS phase. Dou et al. [27] chose PVDF/PS/HDPE blends

Table 1 Interfacial tension of polymer pairs and spreading coefficient of ternary blends at 200 ℃.

Interfacial tension (mN/m)	Spreading coefficient (mN/m)
$\gamma_{PVDF/PS}$ = 4.7	$\lambda_{PS/HDPE}$ = 3.8
$\gamma_{PS/HDPE}$ = 3.4	$\lambda_{PVDF/PS}$ = −13.2
$\gamma_{HDPE/PVDF}$ = 11.9	$\lambda_{HDPE/PVDF}$ = −10.6

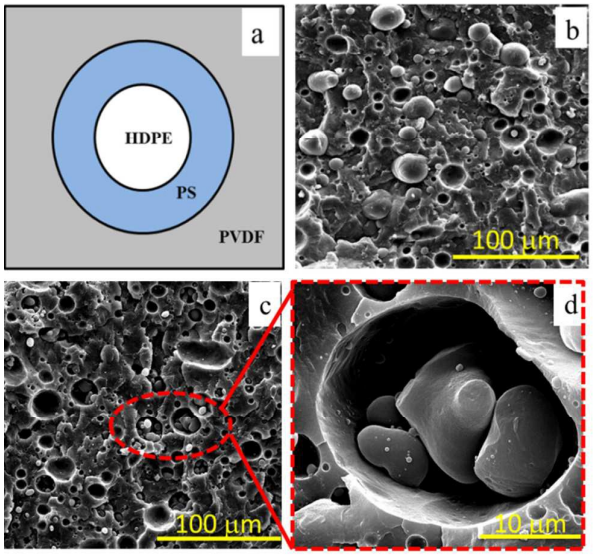

Fig. 2 The core-shell structure of PVDF/PS/HDPE (70/20/10 vol%) ternary blends (a) schematic representations, (b) SEM micrograph of cryo-fractured surfaces, (c) and (d) SEM micrograph of cryo-fractured surfaces with PS etched by xylene.

to prepare a ternary continuous structure, in which the PS engulfed the HDPE phase completely. Therefore, SEM micrographs confirm that a core-shell structure has been formed, where PS is the shell and HDPE is the core. Moreover, the SEM results agree well with the theoretical prediction.

Dispersion of MWCNTs in PVDF/PS/HDPE ternary blends

It is well accepted that the selective localization of fillers in the polymer blends are governed by the surface energy of fillers and polymer components, the affinity of fillers to polymers components, and the viscosity ratio of the polymer phases. In theory, the selective localization of nanofillers in the polymer blends can be predicted by wetting coefficient, ω, according to the Young's equation proposed by Sumita et al [28].

$$\omega = \frac{\gamma_{cnt-1} - \gamma_{cnt-2}}{\gamma_{12}} \quad (3)$$

where γ_{cnt-1} is the interfacial tension between CNTs and polymer 1, γ_{cnt-2} is the interfacial tension between CNTs and polymer 2, γ_{1-2} is the interfacial tension between polymers 1 and 2 . When the value, ω, above +1, below −1, and between +1 and −1 mean that CNTs nanoparticles preferentially locate in polymer 2, in polymer 1, and at the interface between two polymers, respectively.

Table 2 The wetting coefficient between CNTs and polymer pairs

Wetting coefficient	ω
PVDF/PS	1.7
PS/HDPE	−2.1
HDPE/PVDF	−1.1

Table 2 shows the wetting coefficient between CNTs and polymer pairs of PVDF/PS/HDPE. The data shows that a thermodynamically stable interaction is the strongest between MWCNTs and PS, which indicates the stable distribution of MWCNTs in the PS phase. In order to observe whether MWCNTs selectively locate in PS phase, selective solvent extraction is first used. Fig. 3 shows the SEM micrograph of (PVDF/PS/HDPE)/MWCNTs (SM_x) blends. As shown in Fig. 3a, there is no residual of MWCNTs in the blends after PS etched at 0.1 vol% MWCNTs loading, which confirms that MWCNTs selectively locate in PS phase. However, a few MWCNTs residual on the surface of HDPE can be observed from Fig 3b, c, and d. As shown in Fig. 3b2, the thickness of PS layer is about 2 μm when the MWCNTs content is 0.3 vol%. While the length of MWCNTs is about 1.5 μm. thus the cracks formed with PS extraction is too narrow to get through for all the MWCNTs.[18] Moreover, the PS layer thickness is so thin that part of MWCNTs across the PS layer and embed the HDPE phase. What's more, the thickness of PS layer will decrease with the MWCNTs content, increasing MWCNTs can be observed on the surface of HDPE core (shown in Fig. 3b, c, and d). Although, the morphologies of SM_x are influenced with the increase of MWCNTs, the blends still present encapsulation structure. TEM observation was carried out to reveal the dispersion of MWCNTs visually at a more microcosmic scale. We can see from Fig. 4, most of MWCNTs selectively dispersed in PS layer and a few MWCNTs locate at the interface between PS and HDPE and some even embed HPDE phase, which consistent with the SEM micro-morphology.[20] What's more, from the TEM images, it further confirms that the core-shell structure has been formed between the PS and HDPE phases.

Electric properties of the composites

The evolution of DC conductivity as a function of MWCNTs content of composites is depicted in Fig. 5. As shown in Fig. 5a, the DC conductivity of VM_y nanocomposites suddenly increased up to twelve orders (10^{12}) of magnitude at 0.5 vol% MWCNTs loading. In

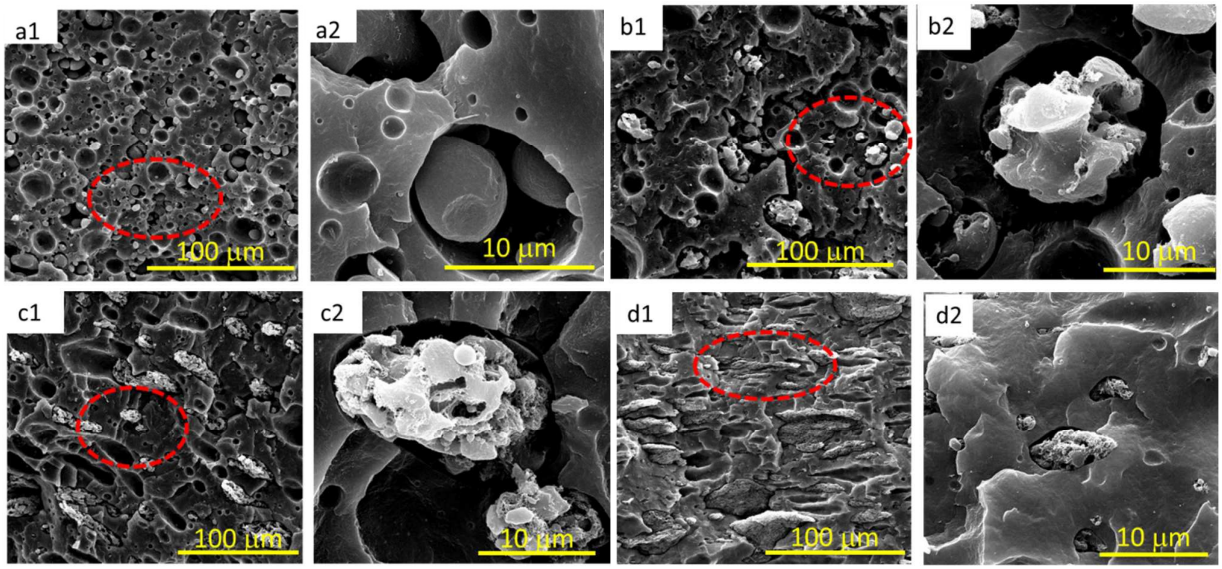

Fig. 3 SEM micrograph of cryo-fractured surfaces of PVDF/PS/HDPE (70/20/10 vol%) blends with PS etched by xylene (a) blends with 0.1 vol% MWCNTs, (b) blends with 0.3 vol% MWCNTs, (c) blends with 0.5 vol% MWCNTs, (d) blends with 1 vol% MWCNTs.

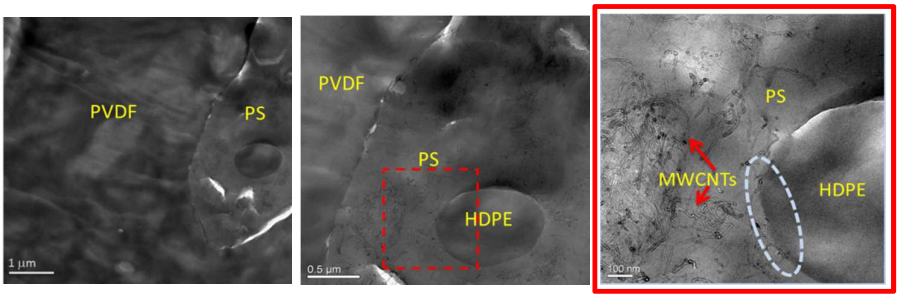

Fig. 4 Typical TEM images of PVDF/PS/HDPE (70/20/10 vol%) blends with 1 vol% MWCNTs.

contrast, the DC conductivity of SM_x nanocomposites increased up to ten orders (10^{10}) of magnitude at 0.5 vol% MWCNTs loading which is presented in Fig. 5b. The conductivity can be further analyzed with the critical content of MWCNTs (φ_c). Above the φ_c, the bulk conductivity of the composites is related with the scaling law, as presented in the equation (4).[17, 29, 30]

$$\sigma_{DC} \infty (\varphi - \varphi_C)^t \text{ For, } \varphi > \varphi_C \quad (4)$$

where σ_{DC} is the conductivity of the composites, φ is the volume fraction of the fillers, φ_c is percolation threshold of MWCNTs, and t is the critical exponent. The best fits straight line was obtained by considering the value for $\varphi_c \approx$ 0.317 and 0.325 vol% for VM_y and SM_x respectively in the log σ_{DC} - log (φ–φ_c) plots, as shown in the inset of Fig. 5.

As we can see, an increase in DC conductivity of the nanocomposites is evident with the MWCNTs loading when its content is less than φ_c value. Meanwhile, it is interesting note that the DC conductivity of SM_x nanocomposites is far lower than that of VM_y nanocomposites at the same loading of MWCNTs. It can be explained in terms of the selective localization of MWCNTs in PS

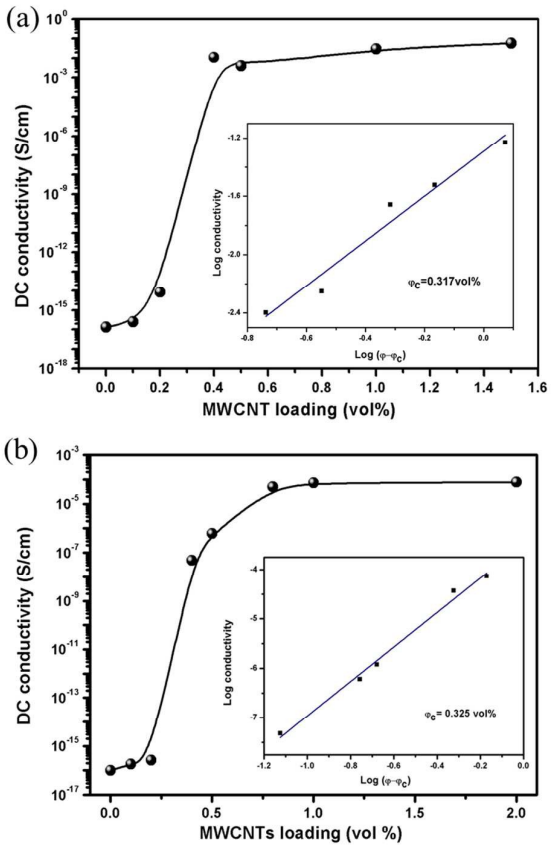

Fig. 5 The evolution of the room temperature DC conductivity of the nanocomposites as a function of MWCNTs loading (a) VM_y nanocomposites, (b) SM_x nanocomposites. Insets show the log-log plots of the conductivity as a function of $\varphi_c - \varphi$ according to eq. (4).

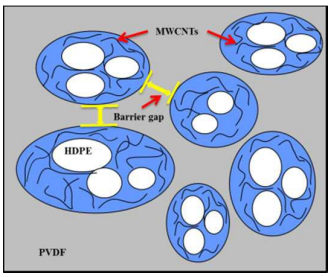

Fig. 6 Illustration of the selective localization of MWCNTs in PVDF/PS/HDPE ternary blends.

shell layer. As shown in Fig. 3 and 4, PS layer intercalates between two insulating layers (PVDF matrix and HDPE core), amounting to introduce the insulating shells on MWCNTs. What's more, the core-shell particles form a segregated structure, and further increase the barrier gap for MWCNTs as shown in Fig. 6. As a result, MWCNTs cannot connect each other directly, which induces the lower DC conductivity of SM_x than that of VM_y composites.

Fig. 7a-b presents the variation of AC conductivity of VM_y and SM_x nanocomposites with various contents of MWCNTs (0.05, 0.1, 0.3, 0.5, and 1 vol%) in the frequency range of 10^2 Hz to 10^7 Hz. As observed, AC conductivity of VM_y and SM_x nanocomposites increases with increasing in the MWCNTs loading. When the

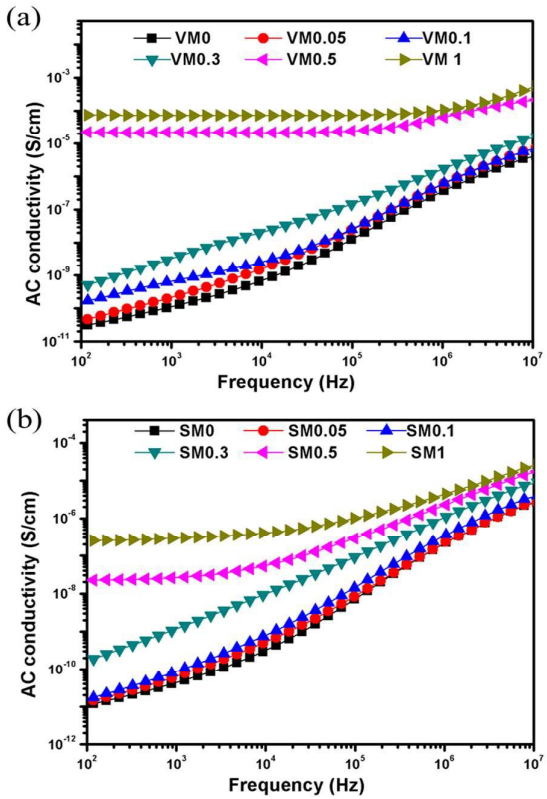

Fig.7 AC conductivity of the nanocomposites with various MWCNTs loading as a function of frequency (a) VM_y nanocomposites, (b) SM_x nanocomposites.

addition of MWCNTs is less than 0.5 vol%, AC conductivity of VM_y and SM_x nanocomposites are almost linearly dependent on the frequency, and showing the typical behavior of an insulating material. It is further noticed that a very drastic change in AC conductivity can be observed with increasing the volume fraction of MWCNTs. A frequency independent platform up to a critical frequency is observed of the composites when 0.5 and 1 vol% MWCNTs incorporated in the blends, implying that the formation of conductive path and shows the character of direct current conductivity.[31] In addition, when 0.5 vol% MWCNTs is added into composites, the AC conductivity of SM_x blends is 10^{-8} far lower than that of VM_y nanocomposites with 10^{-5}, which consistent with the results of DC conductivity.

Dielectric properties of the composites

The good potential of the dielectric materials to store electrical energy is attributed to polarization, which mainly arises from the conductivity mismatch between the fillers and the matrix. According to the Maxwell-Wagner principle, the disparity of the conductivities between two adjacent materials results in polarization and charge accumulation at their interfaces.[29, 32, 33] What's more, two conducting electrodes separated by a dielectric will constitute a capacitor. So the applied electric filed to the nanocomposites will induce the separation and alignment of electric charges, and forming macro-capacitors between adjacent fillers. It has found that the formation of micro-capacitors within matrix was able to generate giant increment of dielectric constant.[34]

The frequency dependence of dielectric constant of the nanocomposites at various MWCNTs contents is investigated at room temperature, and the results are shown in Fig 8. According to Fig 8a-b, the permittivity of nanocomposites increases obviously with the MWCNTs content. It can be comprehended that the amounts of micro-capacitors will increase and the distance between adjacent MWCNTs will decrease with increasing MWCNTs content within a certain range, accumulating vast charges on the interface between two dielectric materials, and then dielectric constant increases rapidly. At low MWCNTs contents, the addition of conductive fillers cannot change the stability of the dielectric constant with the increase of frequency, as seen a frequency-independent behavior. However, when the MWCNTs content is higher than 0.3 vol%, the permittivity of nanocomposites will obviously decrease with the increase of frequency and exhibit a frequency-dependent behavior. This is because the space charges and permanent dipoles cannot keep in pace with the rapidly changing electrical vector as the frequency increases, and they

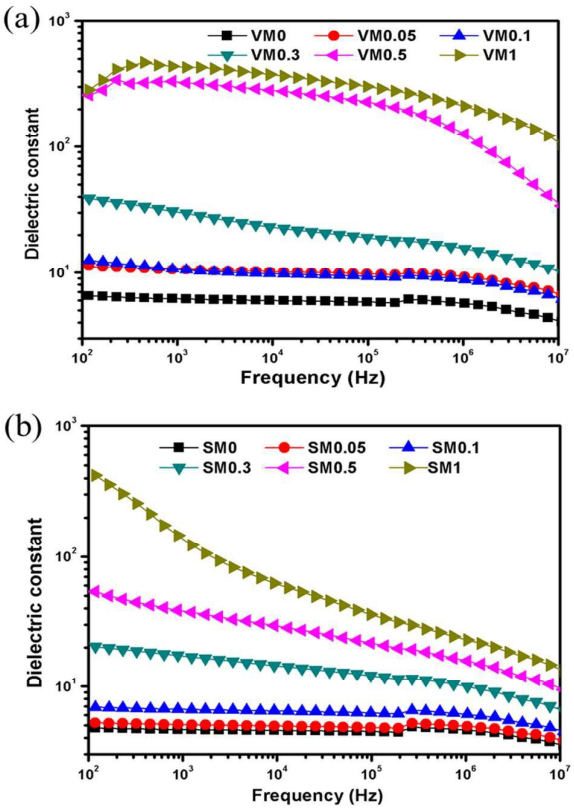

Fig.8 Frequency dependence of dielectric constant of the nanocomposites with different MWCNTs loading (a) VM_y nanocomposites, (b) SM_x nanocomposites.

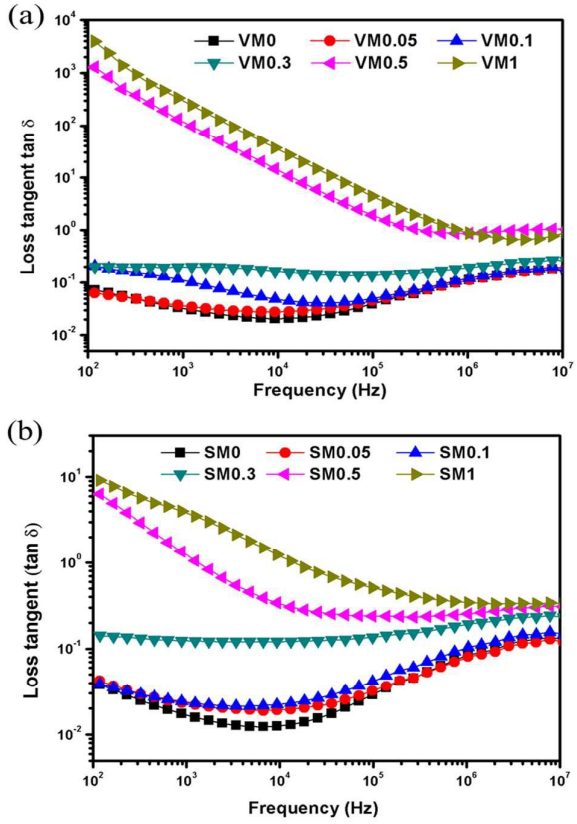

Fig.9 Frequency dependence of dielectric loss tangent (tanδ) of the nanocomposites with different MWCNTs loading (a) VM_y nanocomposites, (b) SM_x nanocomposites.

"relax out" at some frequency. [35] As a result, the effect of overall polarization will decrease, and dielectric constant of composites will decrease consequently.

In general, high dielectric constant is coupled with high dielectric loss for the conductive composites.[29] As depicted in introduction, adding MWCNTs into composites could greatly increase the dielectric constant, however, accompanied by a dramatic increase in dielectric loss. For VM_y nanocomposites, the dielectric loss is only slightly increased when MWCNTs content less than 0.3 vol% as shown in Fig 9a. However, it increases rapidly when MWCNTs content beyond 0.3 vol%. The dielectric loss of VM_y nanocomposites even reach about 4×10^3 with 1 vol% MWCNTs at 100 Hz. We can see from Fig 9b, for SM_x blends, as the content of MWCNTs beyond the percolation threshold (0.325 vol%), the dielectric loss increases quickly with the content of MWCNTs. while, the dielectric loss of SM_x remains at 10 with 1 vol% MWCNTs at 100 Hz, which is 400 times lower than that of VM_y composites. As we know, the dielectric loss of the composites will increase because of the high leakage current caused by the direct connection among conductive fillers. For SM_x blends, MWCNTs selectively distributes in PS shell layer, which prevents MWCNTs from directly connecting each other and induces the low current leakage. As a consequence, a low dielectric loss and high dielectric constant for SM_x composites can be obtained.

Conclusions

The selective distribution of MWCNTs in (70/20/10 vol%) PVDF/PS/HDPE ternary blends have been successfully prepared through melt blending method. The Harkins spreading theory predicts that PS phase will spread over the PVDF/HDPE interface and display a complete wetting behavior. Meanwhile, the wetting coefficient theory predicts that MWCNTs will selectively distribute in PS phase. SEM and TEM images confirm that PVDF/PS/HDPE blends form a core-shell structure, where PS is the shell and HDPE is the core. And the results also demonstrate that the selective localization of MWCNTs in PS layer. It is characterized that the partial electrical network of composites has formed with increasing MWCNTs content determined by the direct current and alternating current conductivity results. The dielectric constant and dielectric loss of composites are strongly dependent on the frequency and MWCNTs content. The dielectric constant of SM_x nanocomposites is as high as 400 with 1.0 vol% MWCNTs at 10^2 Hz, accompanied by a low dielectric loss of 10 which is almost 400 times lower than that of VM_y composites. Therefore, the selective localization of MWCNTs in shell layer of the composites, which display a core-shell structure, is an effective method to reduce the dielectric loss and maintain high dielectric constant simultaneously.

Acknowledgements

The authors gratefully acknowledge the financial support from the National Natural Science Foundation of China (Contract No. 51273219, 51573106 and 51421061), the National Key Basic Research Program of China (973 Program, No. 2012CB025902), the Foundation of State Key Laboratory of Polymer Materials Engineering (Grant No. sklpme2014-3-12) and the Fundamental Research Funds for the Central Universities (No. 2013SCU04A03).

References

1. Y. Shen, Y. H. Lin and C. W. Nan, *Advanced Functional Materials*, 2007, **17**, 2405-2410.
2. Z.-M. Dang, D. Xie and C.-Y. Shi, *Applied Physics Letters*, 2007, **91**, 222902.
3. M. Arbatti, X. Shan and Z. Y. Cheng, *Advanced Materials*, 2007, **19**, 1369-1372.
4. Y. Kobayashi, T. Tanase, T. Tabata, T. Miwa and M. Konno, *Journal of the European Ceramic Society*, 2008, **28**, 117-122.
5. D.-H. Kuo, C.-C. Chang, T.-Y. Su, W.-K. Wang and B.-Y. Lin, *Journal of the European Ceramic Society*, 2001, **21**.
6. M.-F. Yu, O. Lourie, M. J. Dyer, K. Moloni, T. F. Kelly and R. S. Ruoff, *Science*, 2000, **287**, 637-640.
7. P. G. Collins, M. Hersam, M. Arnold, R. Martel and P. Avouris, *Physical review letters*, 2001, **86**, 3128-3131.
8. R. H. Baughman, A. A. Zakhidov and W. A. d. Heer, *Science*, 2002, **297**, 787-792.
9. P. Pötschke, S. M. Dudkin and I. Alig, *Polymer*, 2003, **44**, 5023-5030.
10. Z.-M. Dang, S.-H. Yao and H.-P. Xu, *Applied Physics Letters*, 2007, **90**, 012907.
11. S.-H. Yao, Z.-M. Dang, M.-J. Jiang, H.-P. Xu and J. Bai, *Applied Physics Letters*, 2007, **91**, 212901.
12. Q. Li, Q. Xue, L. Hao, X. Gao and Q. Zheng, *Composites Science and Technology*, 2008, **68**, 2290-2296.
13. X. Zhang, G. Liang, J. Chang, A. Gu, L. Yuan and W. Zhang, *Carbon*, 2012, **50**, 4995-5007.
14. H. Liu, Y. Shen, Y. Song, C. W. Nan, Y. Lin and X. Yang, *Adv Mater*, 2011, **23**, 5104-5108.
15. C. Yang, Y. Lin and C. W. Nan, *Carbon*, 2009, **47**, 1096-1101.
16. Y. Chen, B. Lin, X. Zhang, J. Wang, C. Lai, Y. Sun, Y. Liu and H. Yang, *Journal of Materials Chemistry A*, 2014, **2**, 14118.
17. X. Zhao, J. Zhao, J. P. Cao, X. Wang, M. Chen and Z. M. Dang, *The journal of physical chemistry. B*, 2013, **117**, 2505-2515.
18. X. Zhao, J.-P. Cao, J. Zhao, G.-H. Hu and Z.-M. Dang, *Journal of Materials Chemistry A*, 2014, **2**, 10614.
19. J. Zhang, S. Ravati, N. Virgilio and B. D. Favis, *Macromolecules*, 2007, **40**, 8817-8820.
20. R. Dou, Y. Shao, S. Li, B. Yin and M. Yang, *Polymer*, 2016, **83**, 34-39.
21. R. Dou, C. Shen, B. Yin, M.-b. Yang and B.-h. Xie, *RSC Adv.*, 2015, **5**, 14592-14602.
22. G. Wu, S. Asai and M. Sumita, *macromolecules*, 2002, **35**, 945-951.
23. K. Masenelli-Varlot, G. Vigier, A. Vermogen, C. Gauthier and J. Y. Cavaillé, *Journal of Polymer Science Part B: Polymer Physics*, 2007, **45**, 1243-1251.
24. L. Priya and J. P. Jog, *Journal of polymer science part b: polymer physics*, 2003, **41**, 31-38.
25. S. Manna, S. K. Batabyal and A. K. Nandi, *Journal of Physical Chemistry B*, 2006, **110**, 12318-12326.
26. H. Gramespacher, *Journal of Rheology*, 1992, **36**, 1127.
27. R. Dou, S. Li, Y. Shao, B. Yin and M. Yang, *RSC Adv.*, 2016, **6**, 439-447.
28. M. Sumita, K. Sakata, S. Asal, K. Miyasaka and H. Nakagawa, *Polymer Bulletin*, 1991, **25**, 265-271.

29. Z.-M. Dang, J.-K. Yuan, J.-W. Zha, T. Zhou, S.-T. Li and G.-H. Hu, *Progress in Materials Science*, 2012, **57**, 660-723.
30. D.-X. Yan, H. Pang, B. Li, R. Vajtai, L. Xu, P.-G. Ren, J.-H. Wang and Z.-M. Li, *Advanced Functional Materials*, 2015, **25**, 559-566.
31. M. Monti, I. Armentano, G. Faiella, V. Antonucci, J. M. Kenny, L. Torre and M. Giordano, *Composites Science and Technology*, 2014, **96**, 38-46.
32. D. Taguchi, L. Zhang, J. Li, M. Weis, T. Manaka and M. Iwamoto, *The Journal of Physical Chemistry C*, 2010, **114**, 15136-15140.
33. E. Lim, D. Taguchi and M. Iwamoto, *Applied Physics Letters*, 2014, **105**, 073301.
34. N. Yousefi, X. Sun, X. Lin, X. Shen, J. Jia, B. Zhang, B. Tang, M. Chan and J. K. Kim, *Adv Mater*, 2014, **26**, 5480-5487.
35. Y. Huang, L. Tan, S. Zheng, Z. Liu, J. Feng and M. Yang, *Journal of Applied Polymer science*, 2015, **132**, 7.

Graphical abstract